In-depth characterization of phosphate intercalated Mg Al Layered double hydroxides and study of the PO 4 release properties

Alexandra Jourdain, Christine Taviot-Gueho, Ulla Gro Nielsen, Vanessa Prévot, Claude Forano

In-depth characterization of phosphate intercalated Mg Al Layered double hydroxides to better understand the PO4 release properties

Alexandra Jourdain,[a] Christine Taviot-Gueho,[a] Ulla Gro Nielsen,[b] Vanessa Prévot[a]* and Claude Forano [a] *

Slow-release fertilizers (SRFs) form the core of innovative strategies in sustainable agriculture. Layered Double Hydroxides (LDH), known for their high capacity to sequester plant nutrients, especially phosphate, are emerging as promising candidates for SRF synthesis. The phosphate release properties of MgAl LDH (with a targeted Mg/Al ratio of 2.0) intercalated with HPO_4^{2-} anions were assessed in various aqueous environments. A comprehensive analysis, including in-depth chemical and structural characterizations (ICP-OES, XRD, PDF, 27Al NMR, 31P NMR, FTIR, SEM) of the as-prepared phase unveiled a more intricate composition than anticipated for a pure or ideal Mg_2Al-HPO_4 LDH, encompassing an excess of intercalated phosphate in conjunction with K^+. Beyond the intercalated phosphate, ^{31}P NMR speciation identified multiple HPO42- environments, indicating a portion of the phosphate reacting with intralayer Mg^{2+} to form K-struvite. Additionally, some phosphates were adsorbed onto the surface of amorphous aluminum hydroxide, a side phase formed during MgAl coprecipitation. The phosphate release demonstrated rapid kinetics, occurring within 6 days. Moreover, the released phosphate increased significantly when reducing the Solid/Liquid (S/L) ratio (58%) and further increasing in the presence of carbonate ions (90%). The released phosphate varied from 11.8% to 90% under different release conditions, transitioning from water to a 3.33 mM NaHCO3 aqueous solution at a low S/L ratio (from 20 mg LDH/mL to 0.02 mg LDH/L). The simultaneous release of K^+, Mg^{2+}, Al^{3+} cations indicated the complete dissolution of the K-struvite and partial dissolution of phosphate intercalated MgAl LDH. These results enhanced our understanding of the mechanism governing phosphate release from MgAl LDH, paving the way for potential phosphate recovery by LDH or for the development of LDH-based SRFs.

1. Introduction

Phosphorus is an essential nutrient for plant growth and more than 80% of P extracted from phosphate rocks is used as a fertilizer combined with N and K. However, an excessive administration is necessary to ensure the minimum dose to reach the plant's roots, thus causing a major dissemination and a loss in soils through lixiviation, irreversible precipitation, complexation or adsorption to mineral and organic matter. [1, 2] As a result, chemical systems that can deliver the right dose of nutrients to the plant under kinetic control, have become widely known-as slow-release fertilizers (SRFs) [3, 4].

Most commercially available P fertilizers are based on highly soluble phosphates, embedded or coated with a natural or synthetic polymer matrix that dissolves under a controlled regime [5, 6]. However, most of these polymers are not biodegradable, thereby increasing the microplastic pollution. Alternatively, phosphate minerals with low solubility, such as struvite, have been commercialized. Struvite precipitation from wastewaters with high phosphorus content, is a way to recover orthophosphate as a recycled N-P-fertilizer [7, 8] but this method requires a supply of Mg^{2+}.

Loading phosphate onto a mineral matrix is a third strategy for preparing SRFs. Among the mineral matrices that have been tested Magnesium oxide [9] and hydroxide [10], ferrihydrite [11, 12], clay minerals [13-15]), Layered Double Hydroxides (LDH) display an intrinsic structural affinity for phosphate due to their unique anion exchange properties. LDH $(M^{2+}_{1-x}M^{3+}_x(OH)_2X_x.nH_2O$, abbreviated as $M^{2+}_RM^{3+}$-X with R=(1-x)/x), are layered materials based on the stacking of positive layers $[M^{2+}_{1-x}M^{3+}_x(OH)_2]^{x+}$, made of edge-sharing octahedra of divalent and trivalent metal cations, intercalated with anions and water molecules $[X^{q-}_x.nH_2O]$. Their high anion exchange capacities (a.e.c.) allow to reversibly load in between 80-130 mg PO_4^{3-} per gram of LDH (i.e. 26-42 mg P/g) depending on the $M^{2+}_RM^{3+}$ chemical composition and the intercalated orthophosphate species ($H_2PO_4^-$, HPO_4^{2-} and PO_4^{3-}) (Table S1). Some studies of orthophosphate loading on LDH reported even higher P loading values through excess surface adsorption exceeding the theoretical a.e.c. [16].

According the chemical affinity of LDH/anions series, CO_3^{2-} > HPO_4^{2-} > SO_4^{2-} > OH^- > F^- > Cl^- > NO_3^- [16], orthophosphates display stronger interactions than most of the inorganic anions.

Phosphate release can be obtained by back-exchange of phosphate under favorable physico-chemical conditions such as high concentration of competing $[A^{x-}]$ anion. While a great number of studies reported the adsorption or removal of orthophosphate by LDH for recovery or environmental depollution purposes [17], few studies investigated the release of phosphate by LDH [15, 18-22] and evaluated their efficiency as P fertilizers [23-30].

Some of these studies investigated phosphate release kinetics under model conditions, using water or carbonate, nitrate, chloride or hydroxide aqueous solutions, often far from environmental conditions [31]. Both anion exchange reaction and LDH dissolution [22] contribute to the mechanism of release. Interestingly, P release time was ten times slower with Mg_2Al-HPO_4^{2-} compared with KH_2PO_4 or monoammonium phosphate (MAP) [25].

In most plant growth trials using LDH as P fertilizers, LDH-PO_4 behave as slow-release fertilizers, optimizing the P bioavailability according to the plant needs [20, 29]. The agronomic efficiency of Mg_2Al-HPO_4^{2-} was also confirmed for wheat (Triticum aestivum) [25] for which biomass production after 30 days of growth in tropical oxisoil was similar to that for wheat growth under KH_2PO_4 and MAP. Agrosystems treated with LDH revealed a higher phosphate content in the soil for a longer time, persisting even after rainfall [25, 32]. These recent studies highlight the interest of LDH-PO_4 as slow release fertilizers. However, a better understanding of their controlled-release properties based on Phosphate/LDH interactions could help to increase their efficiency. More specifically, phosphorus release by LDH-PO_4 appears to be highly dependent on pristine LDH materials and on physico-chemical conditions used. In this study, various release conditions in solution (such as pH, solid/liquid ratio, release solution) were explored in order to kinetically control the leaching of P by Mg_2Al-HPO_4^{2-} and link PO_4 release to in-deep characterization of the structure of pristine LDH.

2. Experimental methods

2.1 Chemicals

$MgCl_2{\cdot}6H_2O$, $AlCl_3{\cdot}6H_2O$, K_2HPO_4 and NaOH used for the material synthesis were of reagent grade and purchased from Sigma-Aldrich.

2.2 Samples preparation

Mg_2AlCl-LDH synthesis. A Mg_2AlCl LDH with a targeted Mg(II)/Al(III) molar ratio of 2:1, was synthesized by coprecipitation at a constant pH=10.0 following the procedure described in a previous work [33], except that synthesis was scaled up to prepare about 500 g of LDH in one batch (supporting information S1). This large quantity was produced for crops trials.

Preparation of phosphate-loaded Mg2Al LDH by anion exchange reaction. As described in a previous work, [34]. 800 mL of K_2HPO_4 solution were added to a suspension of 200 g of powdered Mg_2AlCl LDH in 2.2 L deionized water (molar ratio HPO_4^{2-}/Al^{3+} = 1.0, pH = 9.0) and vigorously stirred during 6 h under N_2 atmosphere. The solid phases was centrifuged and washed thrice with deionized water. The solids were dried at 40°C overnight–and milled to obtain a fine powder. The exchanged Mg_2AlCl LDH will be referred as Mg_2AlP.

2.3 Characterization techniques

XRD data were collected on a Philips X'Pert pro diffractometer equipped with a X'celerator 1D detector (2.122° active length), using CuKα1/ Kα2 source in Bragg Brentano θ-θ geometry from 5 to 90°(2θ) with a scan step of 0.016°. DIFFAX software was used to simulate the Mg_2AlP XRD pattern for the identification of XRD data. The simulations of XRD patterns based on the unit cell parameters and the space group were performed using the Le Bail method [35] with FullProf suite package [36]. The atomic Pair Distribution Function (PDF) were obtained from X-ray total scattering data collected on a PANalytical Empyrean diffractometer equipped with a solid state GaliPIX3D detector, a focusing X-ray multilayer mirror, and an Ag anticathode ($K\alpha_1$ = 0.5594214 Å, $K\alpha_2$ = 0.5638120 Å). PDF analysis protocol and results are described in Supporting Information.

The ATR-FTIR spectra were recorded with a Thermo Nicolet 5700 spectrometer (Thermo Fisher Scientific, USA). Thermogravimetric analysis (TGA) were obtained with a Setaram 92-16.16 instruments (France), at a heating rate of $5°C{\cdot}min^{-1}$ under air atmosphere. Scanning electron microscopy (SEM) and Transmission electron microscopy (TEM) images were recorded using respectively a JSM-7500F Field Emission Scanning Electron Microscope operating at an acceleration voltage of 3 kV, and a JEOL JEM2100Plus microscope operating at 200 kV. C, H, N, S elemental analyses were realized using a CHNS/O Thermo Scientific FLASH SMART (Thermo Fisher Scientific, Germany). Solid state ^{27}Al and ^{31}P MAS NMR spectra were recorded at 11.7 T on a JEOL ECZ500CR 500 MHz NMR spectrometer (Japan) using a 3.2 mm double resonance MAS NMR probe with 14 kHz spinning speed. The quantitative ^{27}Al and ^{31}P and NMR spectra were referenced to a 1.0 M solution of $AlCl_3$ ($\delta_{iso}(^{27}Al)$ = 0 ppm) and concentrated phosphoric acid (85% H_3PO_4; $\delta_{iso}(^{31}P)$ = 0 ppm). Analysis of the spectra were performed using ssNake software [37].

LDH matrices composition and supernatants concentration of Mg, Al, P and K were determined by ICP-OES using ICP-OES 5800 Agilent (USA). The solid samples were solubilized using the mineralization protocol described in Supporting information. For release experiments, quantification of phosphate in solution was performed by colorimetry dosage with the phosphoantimonyl-molybdenum blue complex method (λ = 880 nm) using a TECAN-Magellan robot (EVO® Tecan (Switzerland) platform with robotic arm, 4 needles (capacity 5 to 950 µL)), microplate shaker, cryostat) with a Safire II® Tecan 96-wells microplate reader. All the experiments were performed in triplicate.

2.4 Experiments and modelling of release kinetics

Phosphate release kinetic experiments–were carried using 20 mg of Mg_2AlP. Each of the tubes was filled with deionized water (pH = 8.0 ; V = 2.0 mL or 50.0 mL). The tubes were shaken for 9 different periods of time (t = 1, 2, 3, 6, 10, 15, 20, 25 and 30 days) under air atmosphere then solids and supernatants were separated by centrifugation. The solid residues were dried at 40 °C for further characterizations. The release percentage is defined as the ratio of the desorbed P relative to the P content loaded in the parent LDH. Release experiments were repeated 3 times. For each phosphate release curve, the data were modelled using the common kinetic models (Table S2).

Release as a function of the solid/liquid ratio [S/L]. The release amount was measured as a function of the solid (mg LDH)/liquid (volume of deionized water) ratio ([S/L] = 0,02 to 20 mg/mL). Mg_2AlP suspensions were shaken at 21°C on a planetary orbital shaker during 6 days. Supernatants and solids were recovered and analyzed.

Release as a function of the pH. In 50 mL tubes, 20 mg of P-LDH were introduced followed by 50 mL of aqueous solution at different pH (2.0, 4.0, 6.0, 8.0, 10.0 and 12.0) adjusted with diluted HCl or NaOH solution. Samples were shaken at 21°C on a planetary orbital shaker during 6 days. Supernatants and solids were recovered and analyzed.

Release as a function of the carbonated environment and soil juice. The experiment on L/S ratio effect was repeated in a 3.33 mM $NaHCO_3$ solution (pH = 8.4). These conditions were previously used to simulate carbonate content in soil [25]. Another similar experiment was carried out in soil juice. Soil juice was extracted following a reported procedure (see Supporting information) and the chemical composition is reported in Table S3.

3. Results and discussion

3.1 Deep insight of Mg_2AlP structure.

Orthophosphate loading was carried out using an anion exchange reaction at pH = 9.0. At this pH, HPO_4^{2-} is the predominant orthophosphate species in solution (>98%). Analyses performed on Mg_2AlCl by ICP-OES (Table 1) confirms the precipitation of Mg^{2+} and Al^{3+} metal cations from the precursor solution in the expected ratio. The Mg/Al ratio is preserved after the anion exchange reaction with phosphate as expected for a pure topochemical reaction.

Table 1. Chemical analyses of Mg_2AlCl and Mg_2AlP LDH.

$(Mg/Al)_{expected}$	Molar ratio	$(Mg/Al)_{ICP}$	$(P/Al)_{expected}$	$(P/Al)_{ICP}$	K/Al	$(H_2O)_{TGA}$ (245°C)
2.00	Mg_2AlCl	2.14	-	-	-	14.6 %
2.00	Mg_2AlP	2.13	0.50	0.64	0.17	19.8 %

Despite a thorough washing of Mg_2AlP, an excess of phosphorus (28 %) compared with the expected amount from a.e.c. was measured in Mg_2AlP, jointly with K^+ cation (K/Al = 0.17). On the other hand, the hydration content measured by TGA at T=245°C (adsorbed and intercalated water molecules) (Table 1) was higher for Mg_2AlP than for Mg_2AlCl. These results indicate that the Mg_2AlP sample contains not only phosphate ions but also hydrated potassium ions, as described in the case of motukoreaite-type phase containing sodium/sulfate ions ($Mg_6Al_3(OH)_{18}[Na(H_2O)_6][SO_4]_2{\cdot}6H_2O$) [38]. Consistently with the formation of a layered matrix, SEM images showed a comparable platelet-like morphology before and after phosphate intercalation. The preservation of particles morphology during anion exchange is also in good agreement with a topochemical reaction (Figure S1).

From structural point of view, the diffractogram of the precursor Mg_2AlCl (Figure S2) can be indexed in a three-layer rhombohedral $3R_1$ polytype (01*l* reflection with *l* = 2,5,8) typical of stacked $[Mg_{1-x}Al_x(OH)_2]^{x+}$ LDH layers [39]—although broad character of 01*l* reflections indicates intergrowth with $2H_1$ polytypes [40].

After anion exchange with phosphate, the basal spacing deduced from the position of the first reflection on the XRD patterns expands from 7.66 Å (Mg_2AlCl) to 9.30 Å (Mg_2AlP) while the position of the 110 reflection related to the distance between cations within $[Mg_{1-x}Al_x(OH)_2]^{x+}$ layer remained unaffected (Figure 1 A). These values are similar to those reported by Benicio et al.. [29]

It should be emphasized that various basal distances ranging from ~8.9 Å to ~11.0 Å have been reported in the literature for phosphate-intercalated LDH based on XRD data. As can be seen in figure 1A, in the present case, it was possible to explain all the reflections observed in particular those located at low angles ($2\theta < 30°$) by considering the formation of 1H polytype with a large unit cell of a= 9.138 Å ($3*a_0$) and c= 9.31 Å in the space group P-3. The formation of 1H polytype is not surprising since polytypes with octahedral interlayer sites are commonly observed with non-planar oxyanions. [41] The strong similarities between phosphate and sulfate anions in terms of size and geometry (thermochemical radii $r(SO_4^{2-})$=258 pm and $r(PO_4^{3-})$=238 pm) [42] leads us to compare our results to that reported for LDH phases intercalated by sulfate SO_4^{2-}, widely studied in the literature. In one hand, LDH-SO_4 phases exhibit different basal spacings and space groups. Mg_2Al-SO_4 LDH reported by V. Constantino et al. [43] and E. Alvarez-Ayuso et al. [44] display basal spacings respectively equal to 8.80 Å and 8.62 Å, similar to the zincowoodwardite $Zn_2Al(OH)_6(SO_4)_{1/2}{\cdot}nH_2O$ mineral, with space groups P-3 and R-3m with a $d_{(003)}$ distance between 8.5 and 8.9 Å. On the other hand, the mineral K-motukoreaite with chemical composition $[Mg_6Al_3(OH)_{18}][(SO_4)_2K].12H_2O$ displays a basal spacing of 10.87 Å.[38, 45] In this phase, the interlayer domains are composed of $[K(SO_4)_2(H_2O)_{12}]^{3-}$ with the intercalated alkali metal cations coordinated by six water molecules in an octahedral arrangement leading to a greater basal spacing (10.87Å).

Recently, the same authors have reported the formation of shigaite-like LDH $[Mn_{0.667}Al_{0.333}(OH)_2][(HPO_4)_{0.222}K_{0.111}]$. [46] In the latter example, excess of phosphate anions are intercalated along with potassium cations in the manner of ion pair resulting in a strong positional and orientational ordering of interlayer species and the formation of superstructure in the xy plane. Structural analogy with Mg_2AlP clearly indicates that we have formed a similar phase i.e. co-intercalated with phosphate anions and K^+ cations, and with an ordering of the interlayer species introducing a tripling of a parameter ($3*a_0$).

From the value of a_0 (3.046 Å) which refers to the parameter of the sub-cell, one can estimate the Mg/Al ratio in the crystalline part of the sample which is close to 2.8. [47, 48]

This result differs from the bulk ratio value determined by ICP-OES (Table 1) and suggests the presence of aluminum-rich secondary phase, and lower theoretical a.e.c..

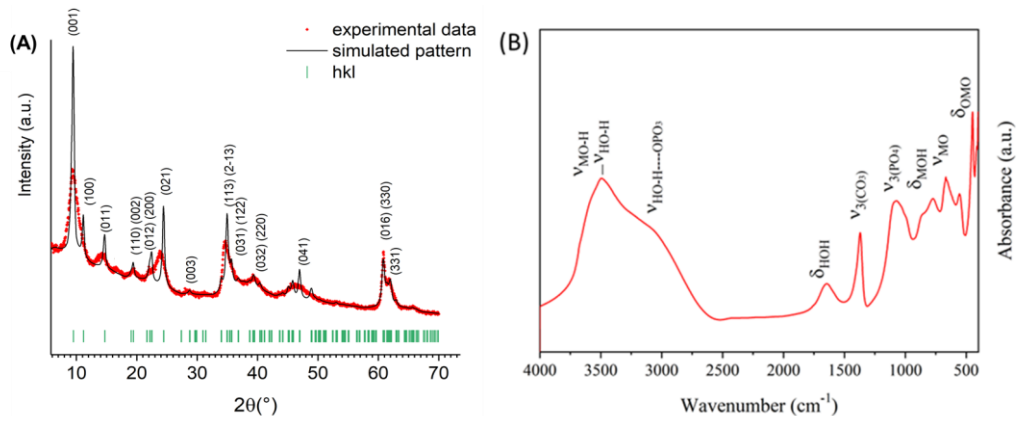

Fig. 1. Powder X-ray diffraction pattern (experimental data (red cross), simulated (solid black line) diagram based on the unit cell parameters a= 9.138 Å and c= 9.31 Å in P-3 space group, Bragg reflections (green ticks) (A) and FTIR spectrum (B) of Mg2AlP

To further investigate the structure of Mg_2AlP sample, the local order was examined by analyzing the pair distribution function (PDF) extracted from X-ray total scattering data. The experimental PDF at low r values (<10 Å) are given in Figure S3. The comparison with Mg_2AlCO_3 (from a previous unpublished study) and Mg_2AlCl as reference samples clearly shows that phosphate intercalation leads to significant changes on the PDF of Mg_2AlP. The distance range examined being limited to the interlayer distance, the peaks observed are mainly from distances within the hydroxide layer plus one interlayer. Most often, in the case of LDH, because of the low contribution of the interlayer species (weak X-ray scattering power and static / dynamic disorder), PDF peaks only reflect the distribution of the distance within the hydroxide layer. In the present case, we clearly observe a contribution of interlayer species which are added to M---OH/M—M pairs. The changes of intensity are observed for P2, P4 and P5 PDF peaks (Figure S3) and could be attributed to atomic pairs involving interlayer species, such as K+ and HPO_4^{2-}/HPO_4^- displaying a high scattering power and located right below Mg/Al cations as illustrated in Figure S4.

Such a greater degree of interlayer ordering is attributed to the partial co-intercalation of K^+ and phosphate leading to strong electrostatic interactions with the hydroxide layers. This explains the interlayer distance and the appearance of supercell reflections in the XRD pattern. Thus, relying on chemical analysis results and XRD characterization and considering the presence of both HPO_4^{2-} and $H_2PO_4^-$ species, it becomes possible to precisely compensate for the positive charge of the layers: $[Mg_{2.8}Al_1(OH)_{7.6}][(HPO_4)_{0.45}(H_2PO_4)_{0.19}K_{0.17},3.2H_2O]$. The strong interactions between the interlayer species and the hydroxylated $[Mg_{1-x}Al_x(OH)_2]^{x+}$ layers enhance the rigidity of the layers. Consequently, the degree of order of the (Mg, Al) $(OH)_6$ octahedra, is increased as shown by the highly resolved FTIR vibrational bands in the 400-1350 cm^{-1} range (Figure 1B and Figure S5). Additionally, hydrogen bond network whose vibrations extend down to 2600 cm^{-1}, is more pronounced compared to Mg_2AlCl. Bands at 1078 cm^{-1} (ν_3) and 987 cm^{-1} (ν_1) correspond to the stretching vibration of the HPO_4^{2-} anion [49]. The intercalation of hydrogenophosphate is confirmed by the presence of two ^1H NMR signals (Figure S6) pointed at 1.1 and 3.6 ppm, in addition to the signal of intercalated and adsorbed H_2O and MOH (4.6 ppm) [50]. This broad signal is attributed to fast proton exchange facilitated by hydrogen bonding between (Mg, Al)O-H and H-O-H.

The ^{27}Al NMR spectra of the chloride precursor (data not shown) and the exchanged phase (Figure 2A) were resolved with two contributions, Al_I and Al_{II}. The Al_I resonance (78.6%, δ_{iso} = 11.31 ppm, C_Q = 1.6, η = 0) arises from Al octahedral sites in the LDH [16, 34]. The second resonance Al_{II} (21.4%, δ_{iso} = 9.54 ppm, C_Q = 2.9, η = 0.5) is assigned to Al environment site in AlOH, amorphous aluminum hydroxide side phase, often formed during LDH fast coprecipitation [34, 51].

The ^{31}P solid state NMR provides additional details on the local environment of phosphate species loaded on Mg_2Al LDH. In data reported in the literature surface adsorption often predominates over intercalation, and when intercalation does occur the structural signature remains ambiguous. This complexity is reflected in the ^{31}P NMR data whose spectra show the presence of several phosphate environments, surface adsorbed, exchangeable intercalated species or precipitated as poorly soluble mineral phases (struvite, bobierrite, cattiite, newberyite, hydroxyapatite).

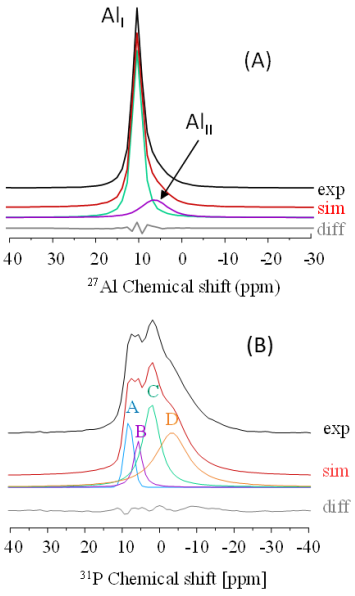

Fig. 2: Experimental ^{27}Al SSNMR (A) and ^{31}P SSNMR spectra (B) of Mg_2AlP along with simulated spectra showing the different components.

The high sensibility of ^{31}P NMR signal to the local environment, i.e. the site symmetry, the neighboring cations, the binding strength renders even more difficult the signal assignment even with the help of referenced phosphate systems (Table 2). ^{31}P NMR data reported for orthophosphate containing MgAl LDH are few (Table 2). They all reveal the presence of different phosphate sites with chemical shift range of frequency from -22 ppm to 14 ppm.

The ^{31}P NMR spectrum of Mg_2AlP (Figure 2B) shows four different environments of phosphorus atoms (sites A, B, C and D). Chemical shifts are typical of orthophosphate anions intercalated or adsorbed on MgAl LDH (Table 3). These four resonances were also observed in our earlier studies of Mg_2Al-LDH after phosphate exposure prepared under similar conditions[34]. However, correlation with PXRD data demonstrates that Mg2AlP local structure is consistent with the presence of a motukoreaite-like phase containing supplementary species ($HPO_4^{2-}/H_2PO_4^-/K^+$).

Site A, resonance at 8.2 ppm was assigned (Table 3) to the intercalated HPO_4^{2-} anion. In this present case, the ^{31}P signal is shielded compared to literature, since it is involved in a motukoreaite-like environment linked with K^+ ion.

Site B, resonances at 5.8 ppm, was assigned to K-struvite based on reported chemical shift [52] (Table 2). Moreover, K-struvite reflections were identified in the PXRD diffractograms of Mg_2AlP residues after phosphate release experiments (data not shown). A comparison of the different ^{31}P chemical shifts reported for phosphate minerals shows a significant overlap in the chemical shift range and a dependence on the degree of protonation (HPO_4^{2-} *vs.* PO_4^{3-}) and hydration (cattiite *vs.* bobierrite) of the samples (Table 2).

Finally, site C (2.2 ppm) and site D (-3.3 ppm) correspond to Mg_2Al LDH (Lundehøj et al., 2019) and AlOH nanodomains, respectively. Site D assignment agrees with ^{31}P NMR of phosphate adsorbed on the surface of an amorphous aluminum hydroxide according to SSNMR studies of phosphate adsorption on Gibbsite and Boehmite [53, 54]. Loading of HPO_4^{2-} anions leads to a strong chemical modification of the surface properties of the LDH, which is highlighted by the inversion of the zeta potential value: 27 ± 2 mV (Mg_2AlCl) and -20,1 ± 0,4 mV (Mg_2AlP).

Behind the global chemical formula of Mg_2AlP, multi-technique analysis (ICP-OES, XRD, SS-NMR) revealed a more complex mixture. In addition to the MgAl-PO_4 LDH phase ($[Mg_{2.8}Al(OH)_{7.6}][(HPO_4)_{0.45}(H_2PO_4)_{0.19}K_{0.17},3.2H_2O]$), Mg_2AlP is composed of 20% of AlOH (^{27}Al NMR quantification) and K-struvite $KMgPO_4 \cdot 6H_2O$ (10 % of total P and 3 % of total Mg).

Table 2: 31P NMR chemical shift of LDH and mineral phosphate

LDH Phases	δiso (ppm)	Species	Ref
Mg3Al-HPO4	14.5	O3PO-H	[55]
	-22.3	OP(O-Al)3	
Mg2Al/H2PO4	8.7 – 9.1		[16]
	2.4 – 3.4		
	-1.5 – -3.0		
	-8.3 – -9.4	AlOP	
Mg2.33AlPO4	2.75 – 4.87		[56]
	-4.72	Mg3(PO4)2.8H2O bobierrite	
	-7.59	Mg(HPO4).3H2O newberyite	
MgxAl/HPO4 (x=2,3,4)	8.3 – 8.7	intercalated HPO4	[34]
	2.3 – 3.4	Surface adsorbed HPO4	
	-0.7 – -1.9	Surface adsorbed HPO4	
	-5.1 – -7.0	AlOH/HPO4	

Mineral Phases	δiso (ppm)	Species	Ref
Al(OH)3/AlOOH	0	AlO-H---PO4	[53]
	-4	H2PO4 adsorbed	
	-10	AlPO4 amorphous	
Struvite MgNH4PO4.6H2O	5.94	PO43-	[52]
K-Struvite MgKPO4.6H2O	6.2	PO43-	
Mg(HPO4).3H2O (newberyite)	1.9	P(OMg)4	[57]
Mg3(PO4)2.22H2O (cattiite)	1.1	PO43-	[58]
Mg3(PO4)2.8H2O (bobierrite)	4.6	P(OMg)4	[59]
KH2PO4	4.0	PO2(OH)2-	[56]
K2HPO4	11.9 – 10.5 – 9.0	PO3(OH) 2-	This work

Table 3: Lorentzian/Gaussian deconvolution of ^{31}P NMR spectra of Mg_2AlP

Site	Mg_2AlP δ_{iso} (ppm) (Intensity %)	Lorentzian	Gaussian	Assignment
A	8.2 (13)	20	566	Intercalated HPO_4^{2-} in Mg_2Al
B	5.8 (9)	500	0	HPO_4^{2-} K-Struvite
C	2.2 (35)	1000	300	HPO_4^{2-} adsorbed on Mg_2Al
D	-3.3 (43)	2100	0	HPO_4^{2-} adsorbed on $Al_{II}OH$

3.2 Phosphate release properties of Mg_2AlP.

Effect of various solid/liquid ratio (S/L in mg/mL). Variable solid/liquid ratios were used in deionized water (from S/L = 0,02 to 20 mg/mL), as 20 mg of Mg_2AlP in volume from 1 mL to 1000 mL. For S/L = 10.0 mg/mL (Figure 3). The desorption kinetic was recorded over a period of 30 days. After 30 days, 12.3 % of the phosphate was released by Mg_2AlP (i.e. 22.6 mgHPO_4^{2-}/gMg_2AlP), 11.8 % during the first 6 days, and 0.5% more during the following 24 days. With a lower solid concentration (S/L = 0.4 mg/mL) (Figure 3) the delivery percentage increased to 35.5 % of total P (i.e. 65.2 mgHPO_4^{2-}/gMg_2AlP).

The S/L ratio the percentage of phosphate release was multiplied by 2.86 from S/L 10 to 0.4 mg/mL. Whatever the S/L ratio used, kinetics of release are fast, more than 96% of the released phosphate are desorbed in 6 days. The shapes of the kinetic plots are similar. Modelling the desorption kinetic curves using various desorption or diffusion models (zero order, pseudo-first order, pseudo-second order, Elovich, liquid film diffusion, intraparticle diffusion) has been widely used in literature to determine the rate constants and to discuss the mechanisms of desorption. Few attempts were done to model the kinetic plots of phosphate release by LDH matrices. Most papers concluded that either the pseudo-second order (Mg_3Fe-HPO_4^{2-}) [31] or the modified Freundlich (Ca_3Fe-HPO_4^{2-}) [22] models gave the best fits whatever the sorbent/sorbate system. These approaches appear often purely mathematical and physical significance of the results may be far from reality as mentioned in some critical papers [60-62]. Indeed, attempts to fit our data (S/L 10.0 and 0.4 mg/mL) with various models, employing both linear (Figure S7) and non-linear (Figure 3B) equations, led to similar conclusions. Rate constants were determined for pseudo-second order model to be equal to 0.18 days^{-1} and 0.23 days^{-1} for respectively S/L 10.0 and 0.4 mg/mL.

The kinetic study was extended to various S/L ratio (Figure 4A). Up to 58% of phosphate was released for the lowest S/L value 0.02 mg/mL (11,8% for the highest S/L=20 mg/mL). A significant variation that points out the major impact of S/L parameter on the phosphate release behaviour of LDH.

Effect of release solutions. P release was also evaluated for Mg_2AlP in contact with $NaHCO_3$ solution ([HCO_3^-] = 3.33 mM, pH = 8.4) and soil juice in order to get closer to environmental conditions (Figure 4A). For each S/L ratio, P release amount decreases following the series HCO_3^- > H_2O > Soil juice, reaching maximum values at highly dilute concentration (S/L = 0.02 mg/mL), 89%, 58% and 49% respectively. As expected, carbonate anions force the release phosphate. An investigation of the role of carbonate speciation on the P release has highlighted the effect of the anion competition. P release was increased when using CO_3^{2-} solution was involved instead of HCO_3^- (71 % vs. 47 % and 61 % vs. 31 % at charge ($H_xCO_3^{-(2-x)}$)/charge (HPO_4^{2-}) respectively equal to 25 and 5, with S/L=10mg/mL). These results highlight that exchange of HPO_4^{2-} with carbonate contributes as a part of the overall P release.

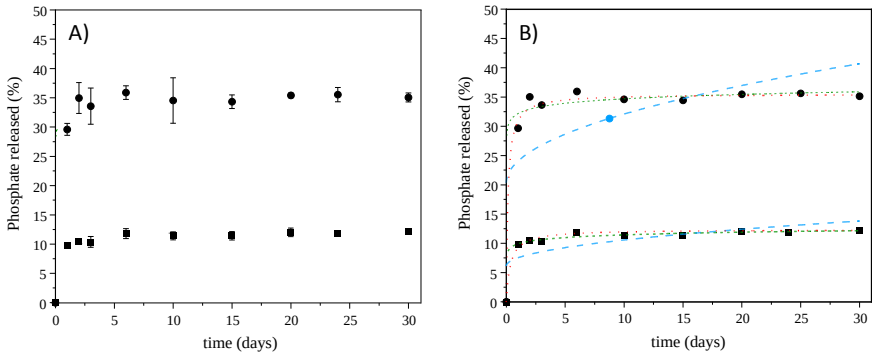

Fig. 3: A) Kinetic of phosphate release by Mg_2AlP at ■ S/L = 10.0 mg/mL ● S/L = 0.4 mg/mL and B) kinetic fitting using pseudo-second order (….), intraparticle diffusion (- - -), Elovich (….) models.

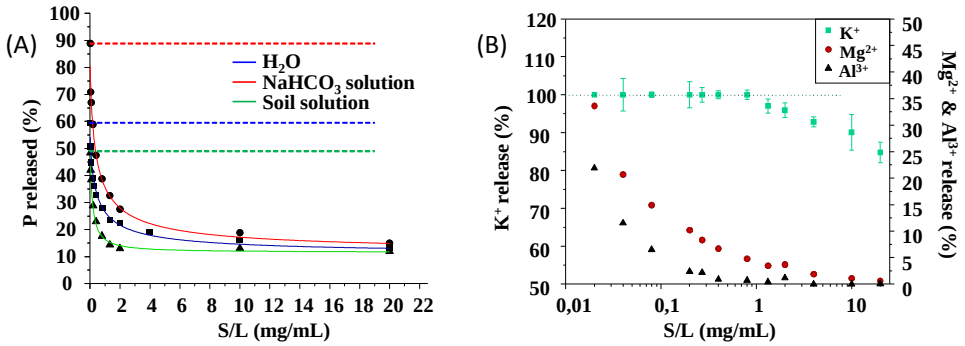

Fig. 4: (A) Kinetic of phosphate release (%) by Mg_2AlP for various S/L ratio (21°C, 6 days contact time) in water solution (blue line), $NaHCO_3$ solution (red line) and soil solution (green line). (B) The percentage of K^+, Mg^{2+}, and Al^{3+} released from the Mg_2AlP- LDH in H_2O as a function of the S/L ratio after 6 days.

Mechanism of P release. The concentrations of K, Mg and Al were determined by ICP-OES and solid residues were characterized by XRD and FTIR. K^+ cations originally in Mg_2AlP interlayer galleries and K-struvite, were totally released for S/L ratio < 1 mg/mL (Figure 4B); 85% already at the highest S/L ratio = 20.0 mg/mL. Chemical stability of MgAl LDH is pH dependent [63], the lower the pH the higher the dissolution.

Interestingly, the decrease in the S/L ratio also favors the solubilization of Mg_2AlP, associated with a progressive release of Mg^{2+} and Al^{3+} cations in solution (Figure 4B) up to 35 % or 20 % respectively for S/L = 0.02 mg/mL, while 0.6 % of Mg^{2+} and 0.05 % of Al^{3+} contents were dissolved, whereas for S/L=20.0 mg/mL. Mg^{2+} and Al^{3+} releases followed the same tendency that phosphorus release when Mg_2AlP was immerged in carbonate and soil solutions: HCO_3^- > H_2O > soil juice (Figure S8). Dissolution in soil juice is limited by the presence of non-negligible quantities of Mg^{2+}, $H_xPO_4^{(3-x)-}$ and K^+ ions (Table S3). All these results highlight that solubilization of solid phases (Mg_2AlP, K-struvite) contributes also to the global release of phosphate.

On one side, at high suspension concentration (S/L = 10 mg/mL), the Mg_2Al LDH structure appeared stable over a period of 30 days under release conditions, as supported by XRD patterns (Figure 5A) and FTIR spectra (Figure 5B). The solid residues kept a similar FTIR feature with a constant vibration bands intensities ratio $I(\nu_{3(PO4)}1070\ cm^{-1})/I(\delta_{OMO}\ 450\ cm^{-1})$ equal to 0.60 and an unmodified XRD pattern distances as described above. On the other side, the release experiment had a stronger effect on the and particle size and shape (Figure 5C & 5D). The material evolved from a morphology of hexagonal platelets with narrow particle size distribution (Ø ~ 200 ± 50 nm) to smaller platelets of heterogeneous shape and size, due to a partial dissolution starting from the particle edges. Immersion of Mg_2AlP in a lower S/L ratio has a stronger effect on the Mg_2Al structure and particularly on the interlayer composition. After 6 days of experiment, with 0.04 mg Mg_2AlP/mL, basal spacing of Mg_2AlP residue decreased to 8.6 Å (Figure S9) with an increase of carbon content to 1.70 % (*vs.* 9.3 Å and 0.86 % with S/L = 20 mg/mL).

This highlights the intercalation of carbonate and the anion exchange. The lamellar morphology and the shape of the platelets were maintained over the release experiments (Figure S10). From the XRD data no secondary phase can be identified, however the motukoreaite-like feature at low angles is lost (Figure S9).

In conclusion, the mechanism of phosphate release involves simultaneously the anion exchange of HPO_4^{2-} intercalated in Mg_2AlP by carbonate anion arising from dissolution of atmospheric $CO_{2(g)}$ or present in aqueous solution (eq. 1) and a partial dissolution of mineral matrices, both LDH (eq. 2) and K-struvite (eq. 3). In such basic occurring conditions released Al^{3+} should partly precipitate as amorphous aluminum hydroxide (eq. 4).

$[Mg_{2.8}Al(OH)_{7.6}][(HPO_4)_{0.45}(H_2PO_4)_{0.19}K_{0.17},3.2H_2O] + CO_3^{2-}{}_{aq.} \Leftrightarrow [Mg_{2.8}Al(OH)_{7.6}](CO_3)_{0.5}.nH_2O + 0.64HPO_4^{2-}{}_{aq.} + 0.17K^+$ (eq. 1)

$[Mg_{2.8}Al(OH)_{7.6}][(HPO_4)_{0.45}(H_2PO_4)_{0.19}K_{0.17},3.2H_2O] \Leftrightarrow 2.8Mg^{2+}{}_{aq.} + Al^{3+}{}_{aq.} + 7.6OH^-{}_{aq.} + 0.64HPO_4^{2-}{}_{aq.} + 0.17K^+ + 3.2H_2O$ (eq. 2)

$KMg(PO_4).6H_2O \Leftrightarrow K^+{}_{aq.} + Mg^{2+}{}_{aq.} + PO_4^{3-}{}_{aq.} + 6H_2O$ (eq. 3)

$Al^{3+}{}_{aq.} + 3OH^-{}_{aq.} \Leftrightarrow Al(OH)_3$ (eq.

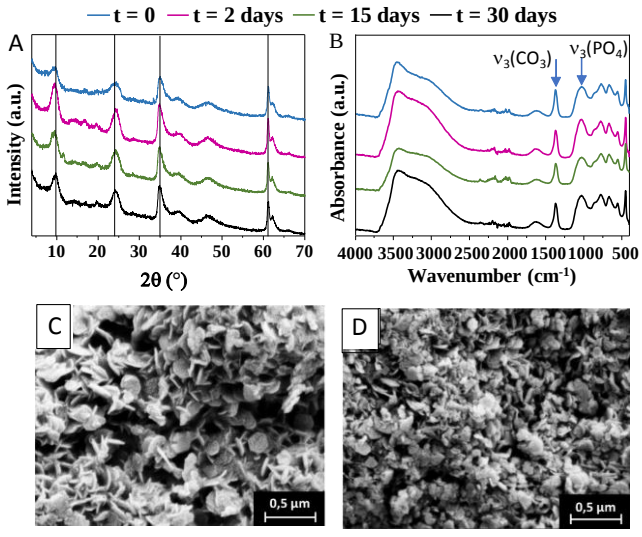

4)

Fig. 5 : XRD (A) and FTIR (B) of Mg_2AlP after release in H_2O at 0, 2, 15, 30 days and S/L = 10 mg/mL. SEM images of Mg_2AlP (C) before and (D) after release in H_2O at 30 days and S/L = 10 mg/mL.

Contributions of anion exchange and dissolution were calculated from Mg/Al/P/K release data (Figure 6) in regard to the global chemical composition and stoichiometry of the inorganic phases for the different S/L ratio tested. At high S/L ratio, almost pure anion exchange mechanism was involved, since dissolution was limited by the concentration. For the lowest S/L ratio (60% of P released), the portion of phosphate released by exchange corresponds to 28 % of P in matrix, 10 % of P sourced from K-struvite ($KMgPO_4$) and the rest of P released
(22 %) are due to LDH matrix dissolution.

A comparison of the phosphate release performances by Mg_2AlP with other $MgAl\text{-}PO_4$ LDH phases reported in the literature is challenging especially due to the limited number of studies and significant variation in experimental conditions, e.g., the choice of LDH, the loading rate, surface adsorption vs intercalation, phase impurities. Indeed, the rate of P release strongly depends on both the LDH/Phosphate interaction and the physicochemical conditions of release. This work demonstrated that total release can be achieved under harsh conditions (high CO_3^{2-} concentrations, low solid/liquid ratio).

This is of great interest for phosphate recovery after sequestration by LDH. However, for fertilization purposes, such extreme conditions are irrelevant, and LDH display limitation in phosphate release as shown on Figure 3 & 6. Similarly, Everaert *et al.*[20] work underlined the same limitations, since using 2mM HCO_3^- solution, $Mg_2Al\text{-}PO_4$ did not release more than 51%.

Effect of pH on phosphate release. Acidity is a major parameter that influences a large number of chemical (phosphate desorption, mineral dissolution…) and physical processes (ion diffusion,…) in soils whose pH range 6.0 – 8.0. These pH conditions may also affect the chemical stability of the Mg2Al LDH matrices and their phosphate release behavior. For example, Benicio et al. [64] reported that release capacities for Mg_xFe and Mg_xAl phases in 2 % citric acid were doubled and quadrupled respectively, compared to release in deionized water. herein the present work (Figure 7A) the P release percentages are reported after suspensions of Mg2AlP in various-pH solutions (contact time 6 days, S/L = 0.4 mg/mL).

At intermediate pH values from 4.0 to 8.0, the buffering effect of the LDH neutralizes the excess of acidity or alkalinity and leads to equilibrated final pH values around pH 8.0 (Figure 7B).

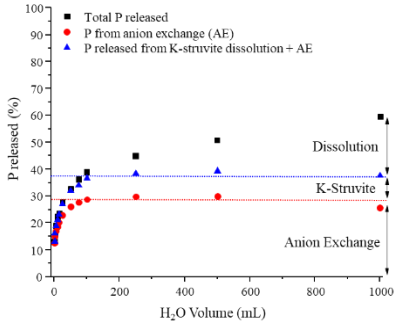

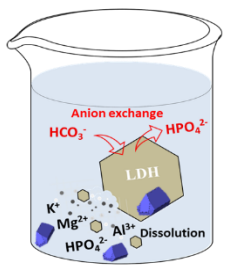

Fig. 6 : Quantification of contributions in Mg_2AlP phosphate release mechanism in deionized water (20 mg Mg_2AlP in V (mL)).

Fig.7 : A) P release percentages of Mg_2AlP at various initial pH (S/L = 0.4 mg/L). B) Evolution of pH under P release.

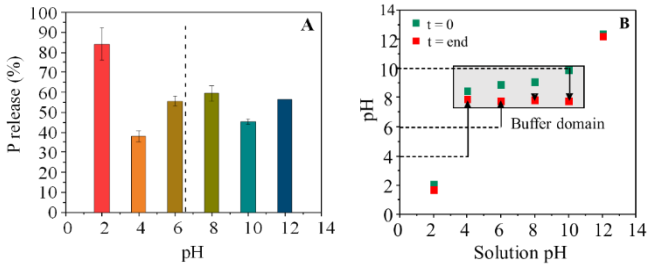

The highest P release content (60 %) is obtained at neutral pH. In such conditions the anion exchange may be considered as the major process as confirmed by the decrease of the basal spacing from 9.4 Å to 7.7 Å (Figure S11A) and the increase in the $I(\nu_3(CO_3)/ I(\nu_3(PO_4)$ FTIR intensity ratio (Figure S11B).

At pH = 2.0, about 85 % of P are released due to a nearly complete dissolution, while at pH = 4 less carbonate is trapped in water compared to higher pH conditions, resulting in a lower portion of dissolved matrix.

Extreme basic pH (12.0) does not affect much the release, confirming that anion exchange with carbonate was driving the release and not the increase of pH (between HCO_3^- and CO_3^{2-} medium) for the experiment in $NaHCO_3$ 3.33 mM.

Conclusion

This ability to immobilize higher amounts of phosphate in LDH than expected, attributed to the presence of K^+ in the interlayer domain, offers significant advantages for the design of K/P SRF formulations. Phosphate-loaded MgAl LDH (69 mg P/g LDH) exhibits tunable and reproducible phosphate release properties that strongly depend on different physicochemical parameters (solid/liquid ratio, ionic strength, carbonate concentration, pH). The P-release rate can vary between 11.8% to 60% in water and may even reach 89% in presence of HCO_3^-. In such conditions, total release is obtained after 6 days. Characterization of the as prepared material and residues collected after release using XRD, SSNMR and FTIR reveals the structural complexity of LDH intercalated by tetrahedral HPO_4^{2-} oxoanions. In addition to the intercalated hydrogenophosphate MgAl-LDH, three other phosphate species have been identified by ^{31}P NMR, in agreement with other analytical data: 1) formation of K-struvite due to a minor hydrolysis of Mg_2Al LDH by HPO_4^{2-}, 2) adsorption of HPO_4^{2-} by amorphous aluminum hydroxide generated during the initial coprecipitation and partial hydrolysis of LDH, 3) a HPO_4^{2-} species intercalated in excess with K^+ cation similarly to the motukoreaite mineral. The kinetics and rate of phosphate release in this LDH are highly dependent on the physicochemical conditions of release, including the

solid/liquid ratio, the presence of interfering ions in the medium, and the pH. The interstratification/contamination by carbonate anions occurring during the release is not reversible and the loss of K^+ reduces the recyclability of the phase under simple conditions. It was noted that, whatever the S/L ratio, the kinetics of release remained quite rapid, and the equilibrium release rate Q_e is reached before the sixth day. Mg_2Al LDH materials, thanks to their high phosphate loading capacity, show great potentiality for a controlled release of phosphate, as demonstrated in a forthcoming paper highlighting their efficiency for wheat growth.

Author Contributions

Alexandra Jourdain : Investigation, Methodology, Wrinting original draft, **Christine Taviot-Gueho** : Investigation, Validation, Writing - Review & Editing **Ulla Gro Nielsen**: Validation, Review **Vanessa Prévot** : Funding acquisition, Conceptualization, Supervision, Writing - Review & Editing and **Claude Forano** : Conceptualization Project administration, Supervision, Writing - Review & Editing.

Conflicts of interest

There are no conflicts to declare.

Acknowledgements

The authors acknowledge the European Regional Development Fund for the funding pf the FERTI+ project and Dr. A. Jourdain salary and the French government IDEX-ISITE initiative 16-IDEX-0001 (CAP 20-25) for supporting the international mobility of Dr. A. Jourdain. Prof. Ulla Gro Nielsen acknowledge The Danish Research Foundation (DFF Grøn Omstilling; grant: 95-305-23601-01130).
The authors acknowledge UCA-Partner for the access to XRD, TEM, TECAN, ICP-OES instruments.

Notes and references

1. A. E. Johnston, P. R. Poulton, P. E. Fixen and D. Curtin, in *Advances in Agronomy*, ed. D. L. Sparks, Academic Press, 2014, vol. 123, pp. 177-228.
2. T. L. Roberts and A. E. Johnston, *Resour. Conserv. Recycl.*, 2015, **105**, 275-281.
3. P. Wang, E. Lombi, F.-J. Zhao and P. M. Kopittke, *Trends Plant Sci.*, 2016, **21**, 699-712.
4. J. S. Duhan, R. Kumar, N. Kumar, P. Kaur, K. Nehra and S. Duhan, *Biotechnology Reports*, 2017, **15**, 11-23.
5. Y. P. Timilsena, R. Adhikari, P. Casey, T. Muster, H. Gill and B. Adhikari, *J. Sci. Food Agric.*, 2015, **95**, 1131-1142.
6. Z. Majeed, N. K. Ramli, N. Mansor and Z. Man, *Rev. Chem. Eng.*, 2015, **31**, 27.
7. M. M. Rahman, M. A. M. Salleh, U. Rashid, A. Ahsan, M. M. Hossain and C. S. Ra, *Arab. J. Chem.*, 2014, **7**, 139-155.
8. B. Li, I. Boiarkina, W. Yu, H. M. Huang, T. Munir, G. Q. Wang and B. R. Young, *Sci. Total Environ.*, 2019, **648**, 1244-1256.
9. Y. Xia, K. Dong, X. Xiang, W. Li, Y. Gong and Z. Li, *Sci. Total Environ.*, 2020, **727**, 138510.
10. Solihin, Q. Zhang, W. Tongamp and F. Saito, *Ind. Eng. Chem. Res.*, 2010, **49**, 2213-2216.
11. L. C. Jessica Bollyn, and Erik Smolders, *Plant Soil*, 2019, **438**, 15.
12. H.-J. Cui, M. K. Wang, M.-L. Fu and E. Ci, *J. Soil Sediment*, 2011, **11**, 1135.
13. R. Borges, Brunatto, S., Leitão, A., De Carvalho, G., & Wypych, F. , *Clay Miner.*, 2015, **50**, 10.
14. R. Borges, S. F. Brunatto, A. A. Leitão, G. S. G. De Carvalho and F. Wypych, *Clay Miner.*, 2018, **50**, 153-162.
15. R. Borges, V. Prevot, C. Forano and F. Wypych, *Ind. Eng. Chem. Res.*, 2017, **56**, 708-716.
16. C. Liu, M. Zhang, G. Pan, L. Lundehøj, U. G. Nielsen, Y. Shi and H. C. B. Hansen, *Applied Clay Science*, 2019, **177**, 82-90.
17. R. Keyikoglu, A. Khataee and Y. Yoon, *Adv. Colloid Interface Sci.*, 2022, **300**, 102598.
18. R. Borges, F. Wypych, E. Petit, C. Forano and V. Prevot, *Nanomaterials*, 2019, **9**, 183.
19. J. Buates and T. Imai, *Applied Sciences*, 2021, **11**, 6489.
20. M. Everaert, R. Warrinnier, S. Baken, J.-P. Gustafsson, D. De Vos and E. Smolders, *ACS Sustainable Chem. Eng.,*, 2016, **4**, 4280-4287.
21. H. Hatami, A. Fotovat and A. Halajnia, *Applied Clay Science*, 2018, **152**, 333-341.
22. M. A. Woo, T. Woo Kim, M.-J. Paek, H.-W. Ha, J.-H. Choy and S.-J. Hwang, *J. Solid State Chem.*, 2011, **184**, 171-176.
23. L. P. F. Benício, F. G. Pinto and J. Tronto, in *Layered Double Hydroxide Polymer Nanocomposites*, eds. S. Thomas and S. Daniel, Woodhead Publishing, 2020, DOI: https://doi.org/10.1016/B978-0-08-101903-0.00017-9, pp. 715-741.
24. S. S. Malhi, Haderlein, L.K., Pauly, D.G., Jhonston, A.M., *Better Crops*, 2002, **86**, 2.
25. M. P. Bernardo, G. G. F. Guimarães, V. F. Majaron and C. Ribeiro, *ACS Sustainable Chem. Eng.,*, 2018, **6**, 5152-5161.
26. M. Everaert, F. Degryse, M. J. McLaughlin, D. De Vos and E. Smolders, *Journal of Agricultural and Food Chemistry*, 2017, **65**, 6736-6744.
27. P. Koilraj, C. A. Antonyraj, V. Gupta, C. R. K. Reddy and S. Kannan, *Applied Clay Science*, 2013, **86**, 111-118.
28. M. P. Bernardo, F. K. V. Moreira and C. Ribeiro, *Applied Clay Science*, 2017, **137**, 143-150.
29. L. P. F. Benício, V. R. L. Constantino, F. G. Pinto, L. Vergütz, J. Tronto and L. M. da Costa, *ACS Sustainable Chem. Eng.,*, 2017, **5**, 399-409.
30. S. Wan, S. Wang, Y. Li and B. Gao, *J. Ind. Eng. Chem.*, 2017, **47**, 246-253.
31. M. Kurashina, T. Amatsu, T. Ochi, N. Ohigashi and E. Kanezaki, *International Journal of Modern Physics Conference Series*, 2012, **6**, 156-161.
32. M. Everaert, R. C. da Silva, F. Degryse, M. J. McLaughlin and E. Smolders, *J Environ Qual*, 2018, **47**, 371-377.
33. K. Charradi, C. Forano, V. Prevot, D. Madern, A. Ben Haj Amara and C. Mousty, *Langmuir*, 2010, **26**, 9997-10004.

34. L. Lundehøj, J. Cellier, C. Forano and U. G. Nielsen, *J. Phys. Chem. C*, 2019, **123**, 24039-24050.
35. A. Le Bail, H. Duroy and J. L. Fourquet, *Mater. Res. Bull.*, 1988, **23**, 447-452.
36. J. Rodriguez-Carvajal, *IUCr Newsl*, 2001, **26**.
37. S. G. J. van Meerten, W. M. J. Franssen and A. P. M. Kentgens, *J. Magn. Reson.*, 2019, **301**, 56-66.
38. A. R. Sotiles, L. M. Baika, M. T. Grassi and F. Wypych, *J. Am. Chem. Soc.*, 2019, **141**, 531-540.
39. C. Forano, U. Costantino, V. Prévot and T.-G. C., in *Handbook of Clay Science*, ed. G. L. Faıza Bergaya, Elsevier Amsterdam, The Netherlands, 2013, vol. 5, ch. Chapter 14.1, pp. 745-782.
40. G. S. Thomas and P. V. Kamath, *Journal of Chemical Sciences*, 2006, **118**, 127-133.
41. A. V. Radha, P. V. Kamath and C. Shivakumara, *J Phys Chem B*, 2007, **111**, 3411-3418.
42. S. J. Louisnathan and G. V. Gibbs, *Mater. Res. Bull.*, 1972, **7**, 1281-1292.
43. V. R. L. Constantino and T. J. Pinnavaia, *Inorg. Chem.*, 1995, **34**, 883-892.
44. E. Alvarez-Ayuso and H. W. Nugteren, *Chemosphere*, 2006, **62**, 155-162.
45. S. Radha and P. V. Kamath, *Inorg. Chem.*, 2013, **52**, 4834-4841.
46. N. A. G. Gomez, A. R. Sotiles and F. Wypych, *Applied Clay Science*, 2020, **193**, 105658.
47. I. Richardson, *Acta Crystallographica Section B*, 2013, **69**, 150-162.
48. A.-L. Troutier-Thuilliez, C. Taviot-Guého, J. Cellier, H. Hintze-Bruening and F. Leroux, *Prog. Org. Coat.*, 2009, **64**, 182-192.
49. Y. Arai and D. L. Sparks, *J. Colloid Interface Sci.*, 2001, **241**, 317-326.
50. P. J. Sideris, U. G. Nielsen, Z. Gan and C. P. Grey, *Science*, 2008, **321**, 113-117.
51. S. S. C. Pushparaj, C. Forano, V. Prevot, A. S. Lipton, G. J. Rees, J. V. Hanna and U. G. Nielsen, *J. Phys. Chem. C*, 2015, **119**, 27695-27707.
52. L. J. Gardner, S. A. Walling, S. M. Lawson, S. Sun, S. A. Bernal, C. L. Corkhill, J. L. Provis, D. C. Apperley, D. Iuga, J. V. Hanna and N. C. Hyatt, *Inorg. Chem.*, 2021, **60**, 195-205.
53. R. Lookman, P. Grobet, R. Merckx and K. Vlassak, *European Journal of Soil Science*, 1994, **45**, 37-44.
54. T. J. Van Emmerik, D. E. Sandström, O. N. Antzutkin, M. J. Angove and B. B. Johnson, *Langmuir*, 2007, **23**, 3205-3213.
55. S. Bougacha Ghorbel, F. Medina, A. Ghorbel and A. M. Segarra, *Applied Catalysis A: General*, 2015, **493**, 142-148.
56. M. P. Bernardo, F. K. V. Moreira, L. A. Colnago and C. Ribeiro, *Colloids and Surfaces A: Physicochemical and Engineering Aspects*, 2016, **497**, 53-62.
57. Y. Du, N. Rees and D. O'Hare, *Dalton Trans.*, 2009, DOI: 10.1039/B909853D, 8197-8202.
58. A. Viani, G. Mali and P. Mácová, *Ceram. Int.*, 2017, **43**, 6571-6579.
59. M. A. Aramendía, V. Borau, C. Jiménez, J. M. Marinas, F. J. Romero and J. R. Ruiz, *J. Solid State Chem.*, 1998, **135**, 96-102.
60. J. Bujdák, *Applied Clay Science*, 2020, **191**, 105630.
61. K. L. Tan and B. H. Hameed, *J. Tawian Inst. Chem. Eng.*, 2017, **74**, 25-48.
62. H. Qiu, L. Lv, B.-c. Pan, Q.-j. Zhang, W.-m. Zhang and Q.-x. Zhang, *Journal of Zhejiang University-SCIENCE A*, 2009, **10**, 716-724.
63. L. Li, E. Warszawik and P. van Rijn, *Adv. Mater. Interfaces*, 2023, **10**, 2202396.
64. L. P. F. Benício, D. Eulálio, L. d. M. Guimarães, F. G. Pinto, L. M. d. Costa and J. Tronto, *Mater. Res.*, 2018, **21**.